On Parameter Bias in Earthquake Sequence Models using Data Assimilation

Arundhuti Banerjee[1], Ylona van Dinther[2], and Femke C. Vossepoel[1]

[1]Department of Geoscience and Engineering, Delft University of Technology, Stevinweg 1, 2628 CN Delft, the Netherlands.
[2]Department of Earth Sciences, Utrecht University, Princetonlaan 4,3584 CB Utrecht, the Netherlands.

Correspondence: Femke C. Vossepoel ([F.C.Vossepoel@tudelft.nl])

Abstract. The feasibility of physics-based forecasting of earthquakes depends on how well models can be calibrated to represent earthquake scenarios given uncertainties in both models and data. We investigate whether data assimilation can estimate current and future fault states, i.e., slip rate and shear stress, in the presence of a bias in the friction parameter. We perform state estimation as well as combined state-parameter estimation using a sequential importance resampling particle filter in a 0D generalization of the Burridge–Knopoff spring-block model with rate-and-state friction. Minor changes in the friction parameter ϵ can lead to different state trajectories and earthquake characteristics. The performance of data assimilation in estimating the fault state in the presence of a parameter bias in ϵ depends on the magnitude of the bias. A small parameter bias in ϵ ($+3\,\%$) can be compensated very well using state estimation ($R^2 = 0.99$), whereas an intermediate bias ($-14\,\%$) can only be compensated partly ($R^2 = 0.47$). When increasing particle spread by accounting for model error and an additional resampling step R^2 increases to 0.61. However, when there is a large bias ($-43\,\%$) in ϵ, only state-parameter estimation can fully account for the parameter bias ($R^2 = 0.97$). Simultaneous state- and parameter estimation thus effectively separates error contributions from friction and shear stress to correctly estimate current and future shear stress and slip rate. This illustrates the potential of data assimilation for estimation of earthquake sequences and provides insight into its application in other non-linear processes with uncertain parameters.

1 Introduction

Earthquake hazard quantification requires estimates and uncertainties of e.g., long-term average recurrence rate of earthquakes. Hence modeling of earthquake sequences may help to understand and forecast the processes that determine these recurrence intervals. Physics-based models of the fault are therefore needed to predict the time when a subsequent earthquake will occur (Barbot et al. (2012)). Using these models, we calculate fault velocity and stresses for the entire earthquake sequence by solving the quasi-dynamic equation of motion with laboratory-derived rate and state dependent friction laws. Most of these physics-based models of seismicity are designed to reproduce general characteristics of earthquakes. To tune and synchronize the model to observed reality Barbot et al. (2012), data assimilation can be useful. Data assimilation combines prior information from simulations of a physics-based model with information in the form of observations to obtain the best possible description of a dynamical system and its uncertainty, (e.g., Evensen et al., 2022). While data assimilation originates from weather forecasting

and oceanography (e.g., Daley, 1997; Bertino et al., 2003; Kalnay, 2003; Vossepoel and van Leeuwen, 2007), few studies have introduced data assimilation for the purpose of earthquake forecasting (e.g., Van Dinther et al., 2019; Werner et al., 2011; Hirahara and Nishikiori, 2019; Hori et al., 2014; Llenos and McGuire, 2011). Applying data assimilation methods using physics-based models to predict the occurrence time of earthquakes is a highly challenging task, because e.g., (i) the governing equations in these physics-based-models may not be sufficiently accurate to forecast the earthquake cycles, (ii) earthquakes generally occur on faults located at depths of several to tens of kilometers and we typically need to rely on indirect and noisy measurements to observe the conditions of the fault, and (iii) the state variables and parameters in the models are highly uncertain and state variables may have multi-modal distributions. Several studies have considered uncertainties in parameters using data assimilation in earthquake-cycle models (e.g. Kano et al., 2010, 2013; Fakuda et al., 2009; Werner et al., 2011). Kano et al. (2013) and Kano et al. (2010) used an adjoint-based data assimilation method to estimate frictional parameters of afterslip. Fakuda et al. (2009) used an Markov Chain Monte Carlo (MCMC)-based method for estimating fault friction parameters. On the other hand, Van Dinther et al. (2019) and Diab-Montero et al. (2022) assumed the frictional parameters to be known and used an Ensemble Kalman Filter Evensen et al. (2022) to estimate the fault states. In our present study, we have used particle filters which is also an ensemble based data assimilation method and is highly efficient for non linear systems with a non-Gaussian prior distribution. Ensemble Kalman filters are not very efficient in encountering non Gaussian characteristics. This is the reason for choosing a particle filter for this study. For a further discussion of available data-assimilation methods, we refer the reader to Evensen et al. (2022). Frictional parameters are important in the evolution of fault slip as they largely determine the recurrence interval of earthquakes. Poorly known or misrepresented parameters can thus introduce a bias, which can be an important source of uncertainty in the model. If this bias is not corrected, the forecasts obtained using the forward model can be misleading. In previous studies, either the frictional parameters have been estimated as part of the data assimilation, or assumed to be perfectly known. In this study, we will investigate the ability of state-estimation methods to correctly update the states and compensate for a parameter bias and we will investigate the ability of state-parameter estimation methods to reduce or even remove it.

The objective of this paper is to evaluate the effectiveness of data assimilation for state estimation and state-parameter estimation in the presence of a parameter bias. To address this, we consider various cases: one set of cases where the parameter is assumed to be known but has a biased value, and one set of cases where we the parameter is estimated along with the state. In these cases, we model fault slip across faults seperating tectonic plates using a spring-slider model, which is assumed to obey a rate-and-state-dependent friction formulation (e.g. Ruina, 1983; Erickson et al., 2008, 2011; Dieterich, 1979). We assimilate observations of fault-slip velocity and fault shear stress using a particle filter to estimate the fault states.

2 Methods

2.1 Data assimilation framework

Let the vector $\mathbf{x}_t$ be the state of a model describing a dynamic system at time index $t = 1, \ldots, T$. We assume that the state is evolving from time $t-1$ to t according to

$$\mathbf{x_t} = M_{t-1,t}(\mathbf{x_{t-1}}, \boldsymbol{\xi}) + \eta_\mathbf{t}, \tag{1}$$

where $\boldsymbol{\xi}$ represents a vector containing the model parameters and $M_{(t-1,t)}$ is the nonlinear operator describing the time-evolution of the system. Here, t is the time step for model integration. Acknowledging that the model is not perfect, we use $\boldsymbol{\eta}_t$ to represent the model error.

Consider a vector $\mathbf{y}$ that contains all observations y_{t_o} at time $t_o = 1, \ldots, T_o$ as $\mathbf{y} = (y_1, y_2, \ldots, y_{t_o}, \ldots, y_{T_o})$. These observations are taken the 'true state' $\tilde{\mathbf{x}}_t$ for each time t_o, which is not necessarily coinciding with the model time steps. Observation y_{t_o} can be related to the true state at that moment as follows

$$\mathbf{y}_{t_o} = H(\tilde{\mathbf{x}_{t_o}}) + \boldsymbol{\beta}_{t_o}, \tag{2}$$

where H is the observational operator that maps the model to the data and $\boldsymbol{\beta}_{t_o}$ is the observation noise error. We assume observational errors to be independent and uncorrelated. Observational errors can be quantified by comparing observations with independent observations for which the measurement error is known, for example from instrument specifications. In the synthetic case presented here, we assume the error statistics to be known. Using these definitions of $\mathbf{x}$ and $\mathbf{y}$, we apply Bayes' theorem to obtain the posterior distribution of the state estimate

$$p(\mathbf{x} \mid \mathbf{y}) = \frac{p(\mathbf{y} \mid \mathbf{x})p(\mathbf{x})}{p(\mathbf{y})}, \tag{3}$$

where $p(\mathbf{y} \mid \mathbf{x})$ is the likelihood, $p(\mathbf{x})$ is the prior density and $p(\mathbf{y})$ the marginal density of the observations that can be considered a normalization factor.

2.1.1 Particle filter

In the following, we describe a data-assimilation method for a generic state vector $\mathbf{z}$, which can represent the state $\mathbf{x}$ of the system, i.e., the variables that change over time, the parameters $\boldsymbol{\xi}$ of the system, which we assume to remain constant, or both. In case of state estimation, the state vector is $\mathbf{z} = \mathbf{x}$ and in case of state- and parameter estimation, the state vector also includes the parameters $\mathbf{z} = [\mathbf{x}, \boldsymbol{\xi}]^\mathrm{T}$.

A Monte-Carlo representation in the form of particles can be used to approximate the posterior PDF $p(\mathbf{z}|\mathbf{y})$ at observation time t_o as

$$p(\mathbf{z}_{0:t_o}|\mathbf{y}_{1:t_o}) = \frac{1}{N} \sum_{i=1}^{N} \delta(\mathbf{z}_{0:t_o} - \mathbf{z}_{0:t_o,i}), \tag{4}$$

where N is the number of Monte-Carlo realizations, with i the counter of these realizations.

We refer to these realizations as particles, while in other studies they may be referred to as ensemble members.

When we insert Eq.4 in Eq.3, and replace $\mathbf{x}$ by $\mathbf{z}$, we obtain an expression for the posterior distribution of the state vector $\mathbf{z}$

$$p(\mathbf{z}_{0:t_o}|\mathbf{y}_{1:t_o}) = \frac{1}{N} \sum_{i=1}^{N} w_i \delta(\mathbf{z}_{0:t_o} - \mathbf{z}_{0:t_o,i}). \tag{5}$$

Here the weights w_i for each particle i are

$$w_i = \frac{p(\mathbf{y}_{1:t_o,i} \mid \mathbf{z}_{0:t_o,i})}{\frac{1}{N} \sum_{i=1}^{N} p(\mathbf{y}_{1:t_o,i} \mid \mathbf{z}_{0:t_o,i})}, \tag{6}$$

where $p(\mathbf{y}_{1:t_o,i} \mid \mathbf{z}_{0:t_o,i})$ is the likelihood belonging to the observations in the time period 1 to t_o. As the observations $\mathbf{y}$ are fixed, this likelihood is a function of the vector $\mathbf{z}$ for each particle i, as discussed in Van Leeuwen (2015). Assuming that the model operator describes a Markov process and the state at a certain (assimilation) time is completely determined by the model operator acting on the state of the (assimilation) time before, we write the weights as

$$w_i = \frac{p(\mathbf{y}_{t_o,i} \mid \mathbf{z}_{t_o,i})}{\frac{1}{N} \sum_{i=1}^{N} p(\mathbf{y}_{t_o,i} \mid \mathbf{z}_{t_o,i})}. \tag{7}$$

The values of the weights are thus determined by the likelihood $p(\mathbf{y}_{t_o}|\mathbf{z}_{t_o})$. Particles with a higher weight are closer to the observation than the ones with a lower weight. For the derivation of this method see Van Leeuwen (2009).

As the number of particles is typically too small to have sufficient samples of the prior, we observe that, as time progresses, most of the particles obtain negligible weights, whereas one or few particles obtain a very high weight. This is commonly referred to as filter degeneracy (e.g., Snyder et al. (2008)).

In the present study, the likelihood $p(y|\mathbf{z}_t)$ that defines the likelihood at a particular time t for observation y_{t_o} is assumed to be given by the Lorentz function

$$p(y_{t_o} \mid \mathbf{z}_{t_o}) = \frac{1}{1 + \frac{[y_{t_o} - H(\mathbf{z}_{t_o})]^2}{\beta_{t_o}{}^2}}, \tag{8}$$

where $\beta_{t_o}{}^2$ is the variance of the observation noise and $\mathbf{z}_{t_o}$ is the state vector at time t_o. The Lorentz function is chosen instead of a Gaussian function as the wider tails leads to less filter degeneracy (Vossepoel and van Leeuwen, 2007). To further avoid degeneracy, we introduce a resampling step known as sequential importance resampling (SIR). This resampling discards particles with very low weights, while duplicating particles with high weight in such a way that the number of particles remains constant. This ensures an approximation of prior distribution that is less sensitive to particle degeneracy. Resampling is performed if the effective sample size N_{eff} exceeds a threshold value. The effective sample size is given as

$$N_{eff} = \frac{1}{\sum w_i^2}. \tag{9}$$

and the threshold is typically chosen to be half the particle size, i.e. $N/2$.

In our study we have implemented a systematic resampling algorithm as it provides better estimates as compared to other resampling methods used in data assimilation [Hol et al. (2006)]. For a description of this and other resampling techniques, see, e.g., Doucet et al. (2001).

2.2 Forward model

2.2.1 Spring-block slider with rate-and-state friction

A simplified, computationally efficient description of earthquake sequences is provided by a spring-block slider system often referred to as the Burridge-Knopoff (BK) model for frictional sliding (Burridge and Knopoff, 1967). Such 0D and 1D models have been shown to retain key features of periodic sequences on homogeneous faults, including quantitative estimates of its recurrence interval and maximum coseismic slip upon using the calculated stress rate from 2/3D models (Li et al., 2021). It simplifies stick-slip motion of a fault caused by the adjacent movement of two tectonic plates using an assembly of springs and blocks (Fig. 1a). The blocks are connected by springs with spring constant k_c and pulled by a plate moving with a uniform velocity V via another set of springs having spring constants k_p. The blocks represent one side of the fault, where the fault line is the contact surface between the blocks and the rough surface the blocks are placed upon. The equation of motion of the ith block in a 1-D chain of blocks of equal mass m is described by (Cartwright et al., 1997, Eq. 1)

$$m\ddot{z}_i = k_c(z_{i+1} - 2z_i + z_{i-1}) - k_p(z_i - Vt) - F_i(\dot{z}_i), \tag{10}$$

where z_i is the position of block i, or the displacement from its initial position, and $F_i(\dot{z}_i)$ describes the frictional force.

We describe the frictional force using a laboratory-derived rate-and-state dependent friction formulation (e.g., Dieterich, 1979; Ruina, 1983; Marone, 1998). This empirical formulation has been used successfully over the last decades to describe the dynamics of sequences of earthquakes, including its spontaneous nucleation, propagation, arrest and postseismic slip in response to tectonic loading (e.g., Lapusta et al., 2000; Lapusta and Barbot, 2012). As in Rice and Tse (1986), the equation of motion (Eq. 10) for rate-and-state dependent friction equations assuming a slip law for the evolution of state variable θ (Ruina, 1983) can be written as (Erickson et al., 2011, Eq. 6)

$$F_i(\dot{z}_i, \Theta) = \sigma_n \left(f^* + \Theta_i + a \ln \frac{\dot{z}_i}{v_0} \right), \tag{11}$$

$$\dot{\Theta}_i = -\left(\frac{\dot{z}_i}{L} \right) \left(\Theta_i + b \ln \frac{\dot{z}_i}{v_0} \right). \tag{12}$$

Here the capital notation Θ refers to $b \cdot \ln \frac{v_0 \theta}{L}$, which is an equivalent yet more convenient description for the rate-and-state friction state variable θ, which can be interpreted as the change in interface strength from reference friction f^* (Nakatani, 2001). Furthermore, σ_n is normal stress, v_0 is the reference velocity assumed to be equal to the plate velocity V below, and a, b and L are the associated rate-and-state friction parameters. After a sudden change in slip rate, parameter a states the direct change of friction. Parameter b describes the evolution towards a new steady-state friction coefficient, where characteristic slip distance L describes the distance taken by state variable θ to reach a new steady-state θ.

In this study, we consider a zero-dimensional (0D) version analyzing a single spring-block slider (Fig. 1a). This model does not take into account the spatio-temporal correlation between different blocks or fault segments. Eq. 10 can be rewritten for a single block for non-dimensional slip of the block with respect to an initial position on the driving plate u (z in Fig. 1) and

non-dimensional slip rate v and solved by assuming $v_p = v_0$. This can be simplified into three partial differential equations written in terms of dimensionless variables (using $\theta = A\hat{\theta}$, $v = v_0\hat{v}$, $u = L\hat{u}$ and $t = \frac{L}{v_0}\hat{t}$, where ˆ indicates the dimensional variables) as (updated from Erickson et al., 2008, Eq. 2)

$$\dot{\Theta} = -v(\Theta + (1 + \epsilon)\ln v), \tag{13}$$

$$\dot{u} = v - 1, \tag{14}$$

$$\dot{v} = -\gamma^2 \left[u + \frac{1}{\xi}(\Theta + \ln v) \right], \tag{15}$$

where $\gamma = \sqrt{\frac{k}{M}}\frac{L}{v_0}$ is the non-dimensional frequency, and $\xi = \frac{kL}{A}$ is the non-dimensional spring constant (see also Gu et al. (1984)). Shear stress τ is derived by multiplying slip with $-\xi$ (e.g., Rice and Tse, 1986).

Finally, internal parameter $\epsilon = \frac{\sigma'_n(b-a)}{\sigma'_n a}$ is a key parameter that measures the sensitivity of the velocity relaxation and includes $A = a\sigma'_n$ and $B = b\sigma'_n$, where σ'_n is the effective normal stress as demonstrated in Erickson et al. (2008).

When compared to a slip weakening friction formulation, the parameter $b - a$ takes the role of a stress drop, while a corresponds to the strength excess (Fig. 1b).

2.2.2 Friction parameter ϵ

To study stick-slip behavior, we limit our 0D model to a velocity-weakening regime for which $a - b < 0$ and the system generates a stable limit-cycle solution with periodic oscillations (Fig. 2). In nature, earthquakes are far from being periodic, but since we have simplified our model to a 0D system and we are not considering the spatio-temporal correlations of the faults, the system generates periodic cycles. The characteristics of the earthquake cycle are strongly influenced by friction parameters a and b. In this study, we address these together and introduce a bias in the prior friction parameter $\epsilon = \frac{b-a}{a}$. The parameter values in this study are based on laboratory experiments by Niemeijer and Vissers (2014) done on phyllosilicate-rich fault rocks, where we select the results representative for depths of 6 km. At this depth, 5 repeat experiments provide a range of plus or minus one standard deviation for $b - a$ from 0.00161 to 0.0077 (Figure 7a in Niemeijer and Vissers (2014)), i.e. equivalent to ϵ 0.161 - 0.77 for a=0.01. In our synthetic perfect model tests, we define $\epsilon = 0.7$ as the true sensitivity of velocity relaxation. Inspired by the measured $b - a$ standard deviations, we selected three cases of parameter bias, i.e., $\epsilon = 0.72$ for a small bias of +3%, $\epsilon = 0.60$ for intermediate bias of -14%, and $\epsilon = 0.40$ for a large bias of -43%. Fig. 2 presents the state trajectories for these three cases. The large impact of the value of ϵ on the system dynamics is evident from the large difference between the trajectory of the simulation with the large parameter bias and that of the true trajectory. All parameters used in the simulations of the 'truth' for the fault slip model are summarized in Table 1.
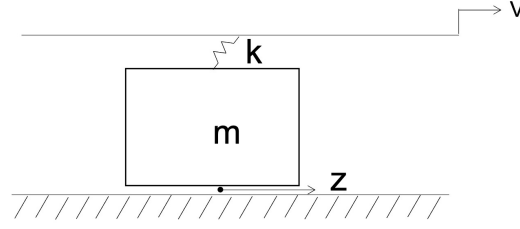
(a)
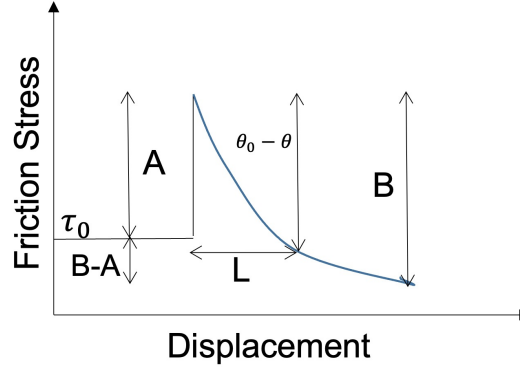
(b)

Figure 1. (a) zero-dimensional (0D) spring block representation used in this study. k is the spring constant, v the slip velocity, z $(= u)$ the slip, (b) Schematic diagram taken from Erickson et al. (2008) illustrating the stress response to a step change in the imposed velocity v of a single spring-block slider model.

3 Numerical experiments

3.1 State and state-parameter estimation for the seismic-cycle model

In state estimation in the seismic-cycle estimation, the state $\mathbf{x}$ to be estimated is given by $\mathbf{x} = [\Theta, \tau, v]^{\mathrm{T}}$. In the state- and parameter estimation, we augment this state vector with:

$$\boldsymbol{\xi} = [\epsilon],$$

where ϵ is the poorly known friction parameter. The state vector is then given by $\mathbf{z} = [\mathbf{x}, \boldsymbol{\xi}]^{\mathrm{T}}$.

By updating this state vector, we update both the state and the parameter at each new analysis time.
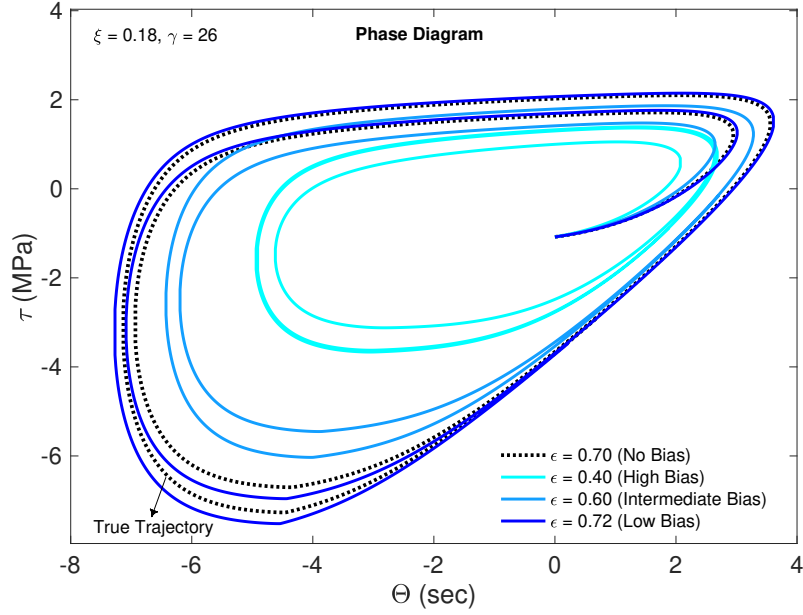
Figure 2. Phase diagram for a Burridge-Knopoff (BK) model with rate-and-state friction formulation when (1) $\epsilon = 0.72$ (a small bias case), (2) $\epsilon = 0.60$ (an intermediate bias case), (3)) $\epsilon = 0.40$ (a large bias case), and (4) the model parameter is equal to the true parameter i.e. a case of no bias.

Table 1. Parameters of the reference model

Parameters	Truth model parameters
Spring constant (k)	10 MPa/m
Period of the analog freely slipping system ($2\pi\sqrt{m/k}$)	5 s
Reference sliding velocity (v_o)	30 mm/yr
Effective normal stress ($\sigma_n{}'$)	120 MPa
Direct effect parameter (a)	0.01
Evolution effect parameter (b)	0.007
Non dimensional friction parameter (ϵ)	0.7
Non dimensional spring constant (ξ)	0.26
Non dimensional frequency (γ)	0.18
Characteristic scale length (L)	80 mm
Friction coefficient (μ_*)	0.60

3.2 Experiment design

In the following, we consider a 'truth run' with ϵ_t and three different priors with ϵ_m: one with a small bias, one with a medium bias, and one with a large bias. To test if data assimilation is indeed capable of estimating the state trajectories, we assimilate synthetic observations of both shear stress and slip rate every 4 time steps. The reason that we assimilate so frequently, is to obtain sufficient information of the behavior of the fault in the short co-seismic phase, i.e., the phase of the earthquake itself. The performance of the data assimilation is evaluated by comparing state estimates to the true trajectory.

3.3 Twin experiments

Since the true state of the fault system is unknown, we validate our data assimilation algorithms using twin experiments. Using these synthetic experiments, we can assess whether data assimilation methods are able to correctly evaluate the posterior distribution of the state. For the synthetic truth we select a forward model run that follows Eq. 13, 14 and 15. The initial conditions of the three state variables are Θ_0, d_0, v_0 = (0,6,1).

For state- and parameter estimation, a different approach has been adopted to generate the prior. As we observe that the state variables are highly sensitive to the parameter value, we make sure that prior state variables are fully consistent with the prior parameter values. For this, we follow the following procedure: (1) We sample N prior parameters ϵ'_m (where N is the number of particles) from a log-normal distribution of std. deviation 0.01 and mean as ϵ_m.

(2) For each $i = 1, \ldots, N$ parameter values, we run the model forward for a small time duration (around 100 time units) using $\epsilon'^{,i}_m$.

(3) We sample the initial conditions of the state variables (Θ, d, v) from these N forward runs at any random time from each trajectory i.

In this way, each state variable and the parameter chosen in the ensemble (Θ_i, τ_i, v_i, ϵ_i) represent a different trajectory, for a different value of ϵ_m. Since each particle has a different parameter value, the prior ensemble contains different recurrence times for earthquake slip events.

Synthetic observations are produced by sampling from the synthetic truth and adding an observational error from a Gaussian distribution with standard deviation σ_β.

3.3.1 Data assimilation settings

The experiments are performed with 1000 particles using a sequential importance resampling (SIR) particle filter. The observations are provided for the two state variables τ and v, as these are most likely to be observable, following the approach and large uncertainties determined in Van Dinther et al. (2019). We sample observations at intervals of 4 time units i.e. $\Delta t = 4$ and add synthetic observational noise sampled from a normal distribution of zero mean and variance $\sigma_\beta{}^2 \sim N(0, \sigma_\beta{}^2)$. Large assimilation steps can adversely affect data assimilation, as they can miss variations in earthquake. Thus, it is necessary to choose a short time step. In the present study, observations were sampled at 4 time units with the standard deviation of observation error as σ_β is 0.6 for fault shear stress and 1.15 for slip velocity observations. These values are consistent with estimates

of Van Dinther et al. (2019) and Mowafy and Bilbas (2016). The stochastic model error η_t (Eq.1) for the state evolution is sampled from a normal distribution $\sim N(0,\sigma_\eta{}^2)$ with $\sigma_\eta = 0.01$. We add a value of 0.01 amplitude to represent model error in the fault shear stress τ and state variable Θ and 0.5 for slip velocity v.

4   Results and analysis

4.1   Case A: State estimation

Figs. 3 (b)-(d) illustrate the evolution of the posterior mean τ (red) and all prior particles (grey) in the three cases of parameter bias and compare it with the reference case of no bias ([Fig.3 (a)]). We refer to the posterior mean as the analysis. When the parameter bias is small, the prior estimates of the fault stress and slip rate evolution capture the truth well as seen from Fig.3 (b). On the other hand, for the case of intermediate (Fig.3 (c)) and large bias Fig.3 (d), the prior state estimation fails to capture the evolution of the shear stress after a few seismic cycles, which complicates the data assimilation going forward. Fig. 2(b) clearly demonstrates that the data assimilation in the large bias case ($\epsilon_m = 0.40$) is unable to account for the difference in state evolution caused by the parameter bias.

To better understand and improve these data assimilation results, we analyze the results for the experiment with intermediate bias in more detail (Fig. 4). By assimilation of data representative of both the interseimic and coseismic periods, we determine whether stress can be estimated. Throughout the paper we illustrate the stress for a number of assimilation times that represent the time epochs before and after an earthquake (Fig. 3a): $t = 16, 20, 24, 72, 76$. In the enlarged version of the figure (Fig. 5), we can see the probabilistic estimate of fault shear stress based on assimilation of coseismic data at $t = 20$. The prior and posterior density represent the particles before and after undergoing resampling respectively. The mean value of the posterior density of stress corresponds better to the true value than that of the prior density. In fact, at time $t = 20$, the particles closest to the observation (representing a pre-slip condition) have the highest likelihood and consequently obtain the highest weights. As a consequence, the posterior density has its peak close to the truth. It should be noted that particles with shear stress values that are farther away from the observations may still obtain high weights because of their fit to the observed slip rate. As a result, the posterior trajectory is close to the observations, but fails to completely follow the true trajectory. Fig. 6 (a)-(j) illustrates this further with phase diagrams, which show by means of scatter plots the distribution of particles in the Θ - τ space. The blue and black line in the phase diagram of Fig. 2(b) represent the trajectory of the particles when the model parameter ϵ_m is 0.60 (intermediate bias) and 0.70 (no bias), respectively.The size as well as the color of the symbols indicate the particle weights. Fig. 7a-j presents the resulting PDF distribution of the corresponding plots in Fig. 6.

The particles with a bias in parameter show a phase difference compared to the truth (Fig. 6a-e). Trajectories of particles with lower values of ϵ have a shorter cycle and their $\Theta - \tau$ trajectories are always ahead of the true trajectories. At time $t = 16$, i.e., in the inter-seismic phase, the particles and the truth are almost in sync. However, at the co-seismic phase ($t = 20$), minor differences in the state for that specific moment can result in large differences in the state trajectory. In this phase, particles that were close to each other previously are pulled apart. After the co-seismic phase, i.e., for $t = 24$, the particles of the biased prior parameter, which have shorter cycles than the truth, reach the inter-seismic phase of the subsequent earthquake event faster

than the truth. After this, the pattern repeats itself. When there is no bias (Fig. 6(f)-(j)), the particles are always in sync with the truth. Compensating for a bias in the prior parameter could also be achieved by changing assimilation settings. In this study, we explore the effect of (i) increasing the model error, or/and (ii) resampling twice rather than once.

Using different assimilation settings, it is possible to inflate the ensemble.

We note that a biased parameter value makes it physically impossible to have Θ and τ in the same phase and amplitude as in the true seismic cycle for an extended period of time. With different assimilation settings, though, it might be feasible to adjust the state such, that we can correctly predict the arrival of the next earthquake. Fig.8a-c shows the state-estimation results for three different data assimilation settings as well as the case of joint state-parameter estimation in Fig.8d. It can be seen from the figure that increasing model error along with frequent resampling leads to a more effective compensation of the biased prior parameter than state estimation without these settings (Fig.3c).
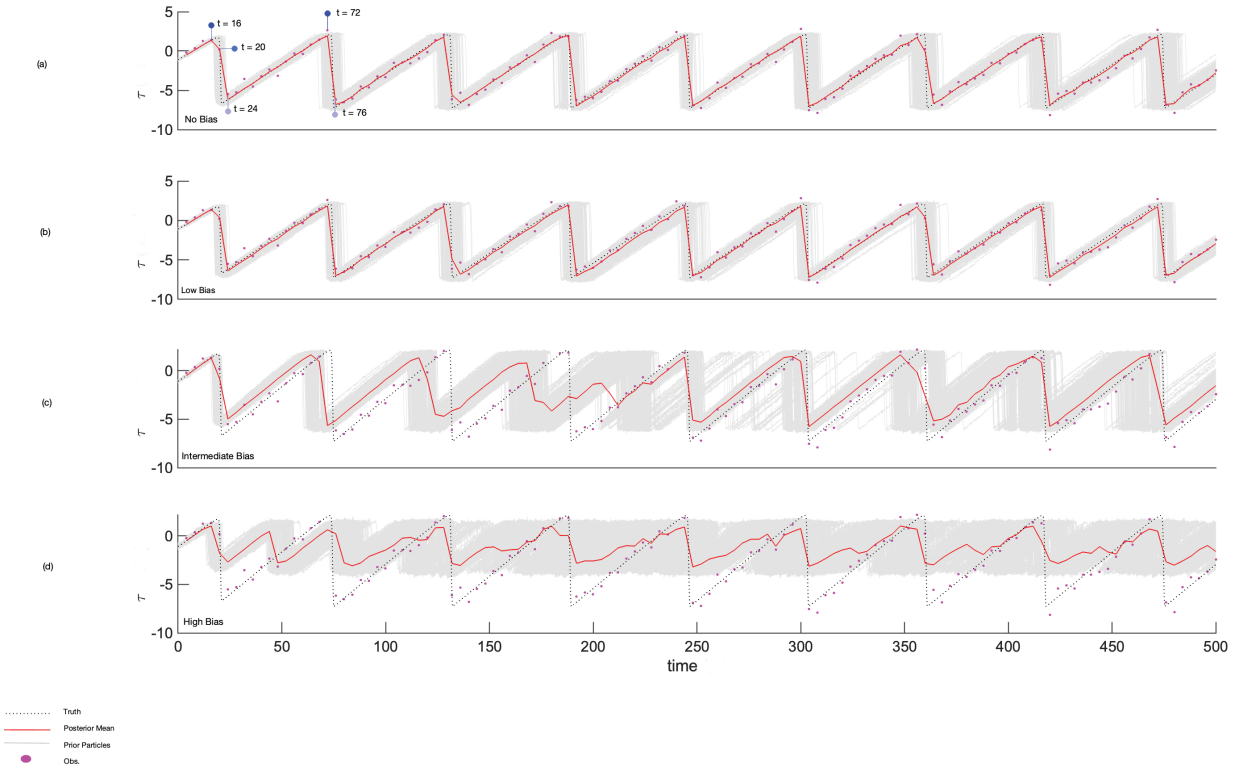
Figure 3. Evolution of 1000 particles along with the posterior mean, observation and truth of state variable τ for state estimation for (a) the case when the model parameter is equal to the true parameter i.e. a case of no bias ($\epsilon_m = 0.70$), (b) a small bias case ($\epsilon_m = 0.72$), (c) an intermediate bias case ($\epsilon_m = 0.60$) and (d) large bias ($\epsilon_m = 0.40$), when $\epsilon_t = 0.70$, $\gamma = 0.26$ and $\xi = 0.18$.
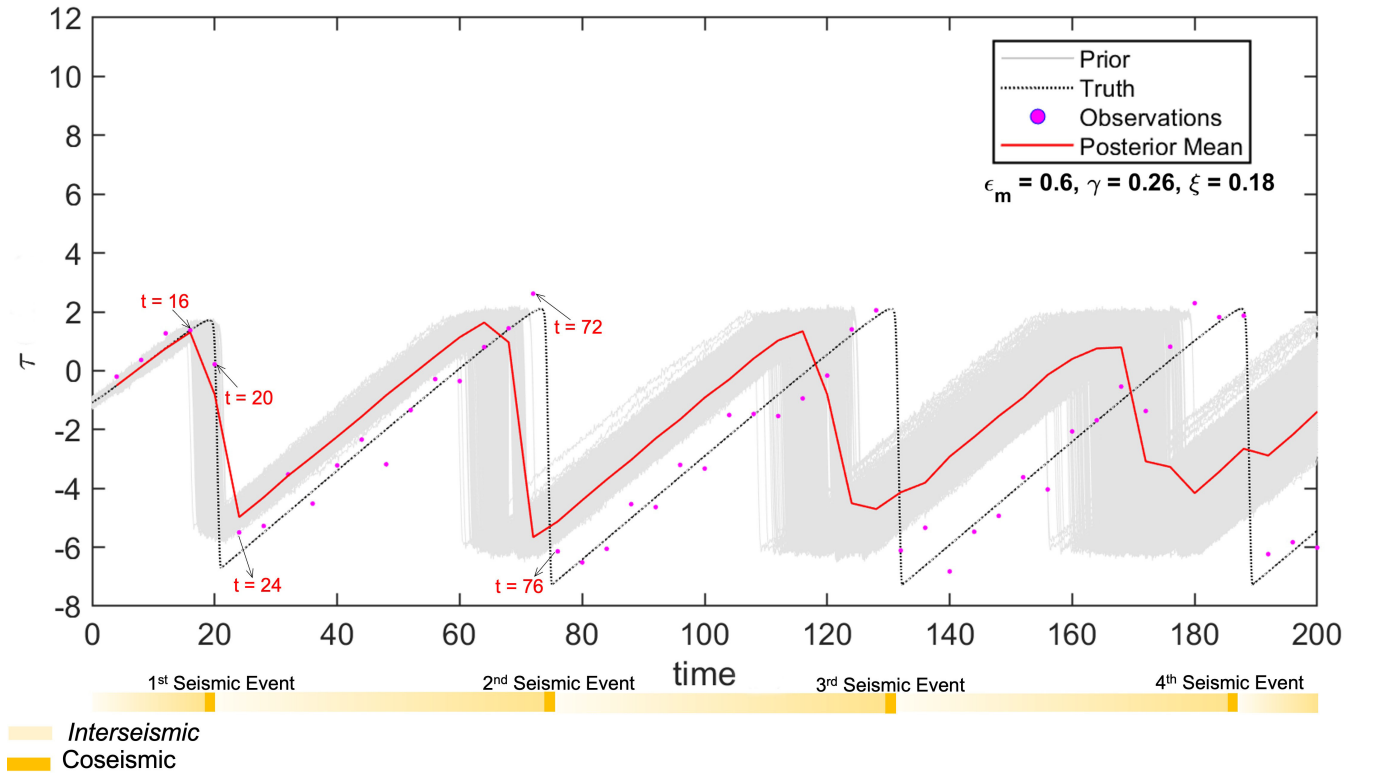
Figure 4. Shear stress evolution. The coseismic and inter-seismic phases in the seismic cycle have been highlighted. The time points discussed in the study are $t = 16, 20, 24, 72, 76$ in the interseismic phase and $t = 20$ in the coseismic phase.
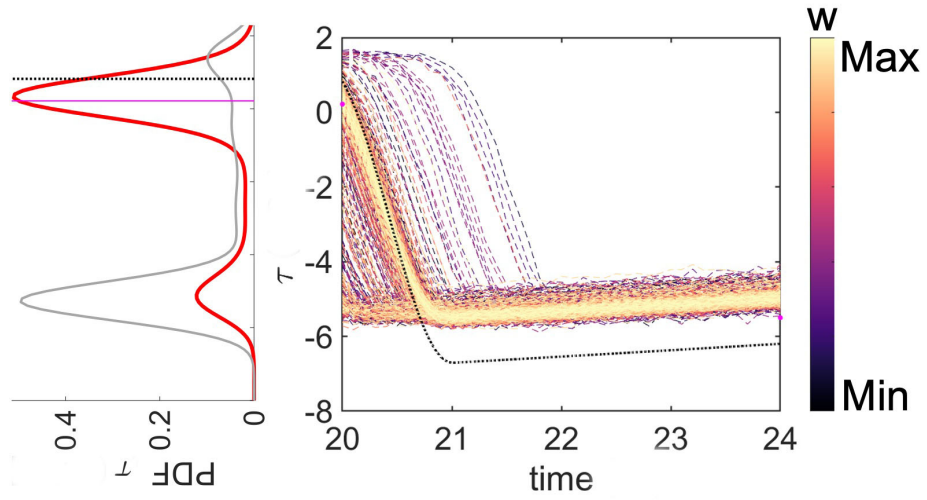
Figure 5. Shear stress evolution with weight distribution at time $t = 20$. The color of the lines represents the value of the weight, which is a function of the distance between the prior shear stress estimate and the observation. The red line represents the posterior pdf, the grey line represents the prior pdf, the magenta line shows where the observation stands, and the black line is the true state.

Stateb estimation (std 0,01)
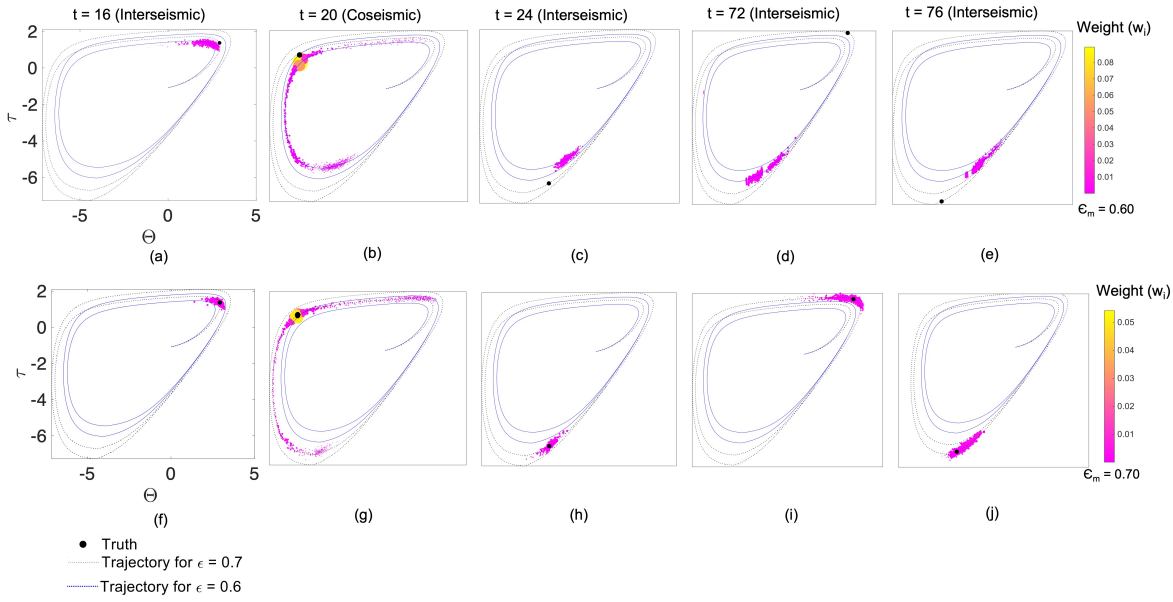
Figure 6. Particles in the Θ-τ space for the case of state estimation with (a-e): intermediate bias ($\epsilon_m = 0.6$) and (f-j) no bias ($\epsilon_m = \epsilon_t = 0.7$). The points represent the particles in the distribution while the lines represent the trajectories in the phase diagram for the respective value of the parameter ϵ_m. The blue line represents the phase diagram for $\epsilon_m = 0.6$ whereas the black line is for the case when $\epsilon_t = 0.7$. The size and color of the symbols representing the particles reflect the weight of each particle.
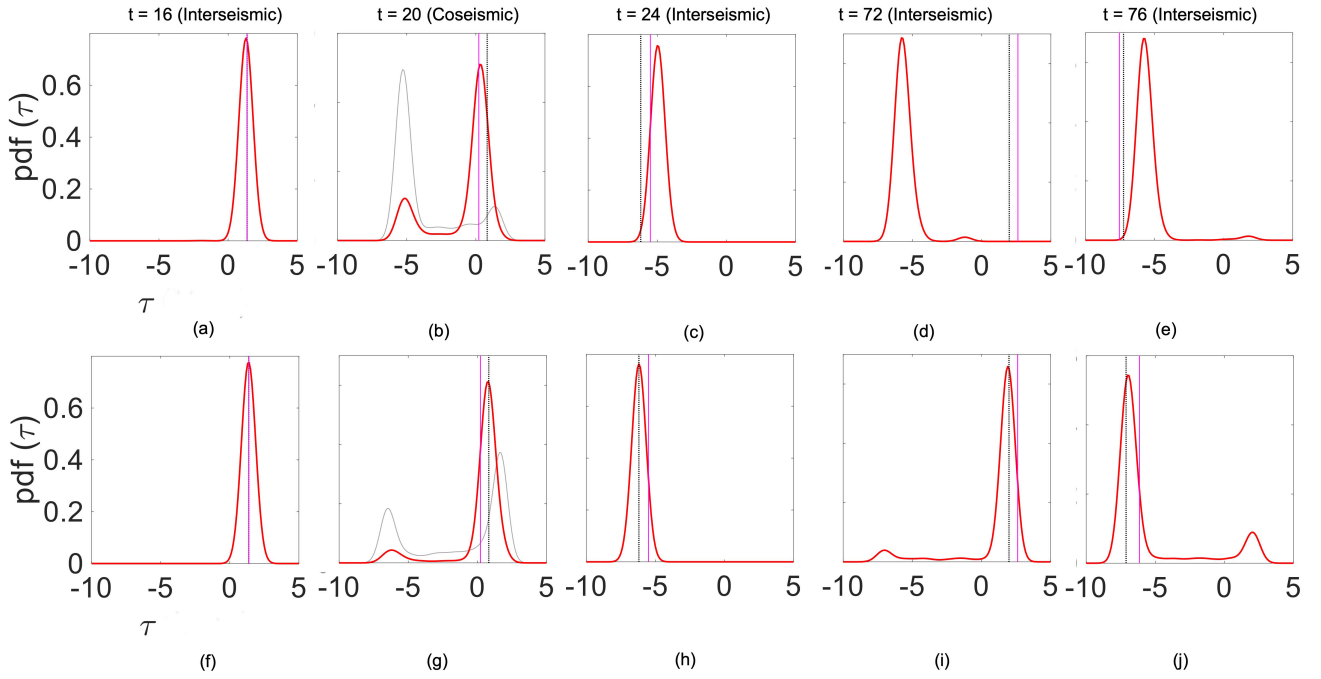
Figure 7. Corresponding PDFs representing the posterior mean in red, prior in grey line, observation in magenta and truth in black line for the case illustrated in Fig.6.
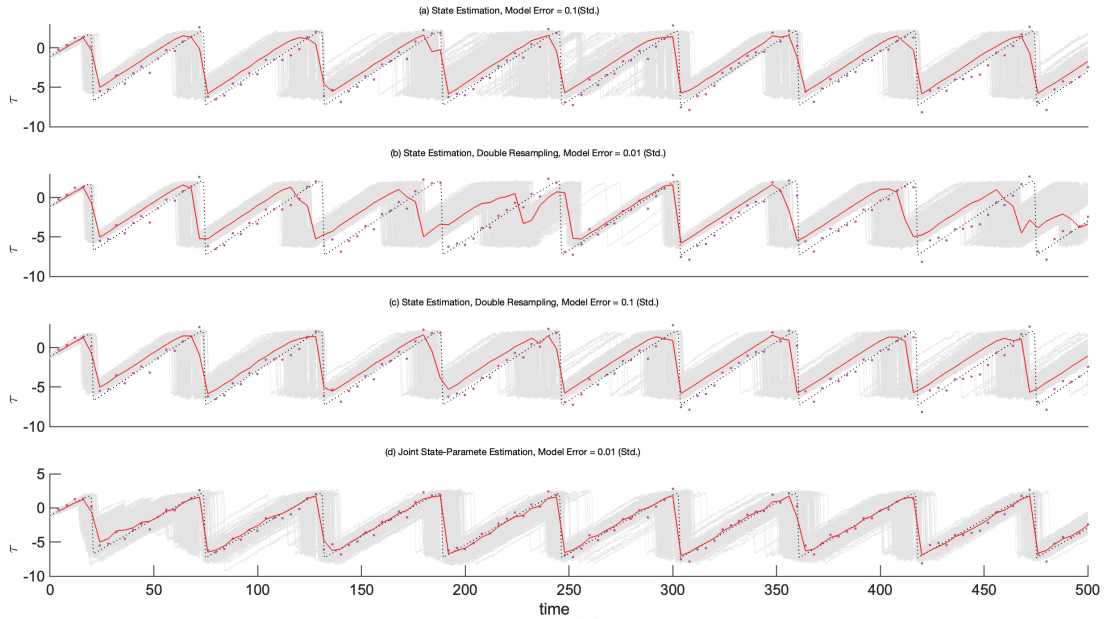
Figure 8. Evolution of particles with time for intermediate bias in state estimation with (a) higher model error ($\eta_t = 0.1$), (b) double resampling ($\eta_t = 0.01$), (c) combination of higher model error ($\eta_t = 0.1$) and double resampling. (d) Joint state-parameter estimation ($\eta_t = 0.01$).

4.2 Case B: Increased model error

255   The model error in the forward-model equation represents the imperfections in the model and thereby maintains ensemble spread. Adding η_t to the forward model equations improves the efficacy of the filter. Choosing a smaller model error reduces the spread, which restricts the solution space considerably.

   We find that inclusion of model error has a noticeable positive effect on the posterior estimate (brings the mean of the posterior closer to the truth) when the parameter bias is either small or intermediate.

260   We observe that increasing the model error causes the prior τ distribution of the particles to have two peaks in the co-seismic phase. This was a single peak when the model error was smaller. This shows that increasing model error allows for a larger variety of states in the prior. The phase diagrams for the intermediate bias case when we increase the model error (η_t in Eq.1) is presented in the supplement figures (Figure S1).

4.3 Case C: Double resampling

265   Resampling improves the effectiveness of the particle filter by introducing more particles with a state close to the observed state 2.1.1. We observe that double resampling retains particles that are in the same interseismic phase as that of the truth as in $t = 24$). From this, we conclude that double resampling can be useful in retaining more particles "in sync" with the truth

in the distribution, but additional spread in the ensemble is required to shift the posterior distribution more towards the truth. It is also important to highlight that in Fig.8b, which represents the double resampling experiment, we observe a double peak at 250 time steps. At this time step, the data assimilation analysis does not fit the observations well. A similar mismatch is observed after approximately 500 time steps in this experiment. At these moments, the double resampling effectively increases the spread in the particles to such an extent, that the constraint to the shear stress observations becomes less strong. Hence, we can conclude that though double resampling can be useful in retaining important particles in the prior distrbution, it is not as effective in increasing the ensemble spread as the increased model error (Fig.8a). The effect of double resampling on the posterior distribution for an intermediate bias is provided in the supplement figures (Figure S2).

4.4 Case D: Increased model error and double resampling

We study the effect of increasing the model error with consequent double resampling on the posterior estimates and use the term 'combined adjustment' for this data assimilation setting. The posterior distribution of stress for the combined adjustment captures the truth distinctly better compared to the case with model error only. There is no significant difference in the forecasting ability of the prior particle distribution in the first seismic cycle for the combined adjustment. Increasing model errors and double resampling both increase variability within the particles. However, at time $t = 76$, after the co-seismic phase, particles of this combined adjustment experiment are no longer fully in sync with the truth. The effect of combined adjustment on the posterior distribution for an intermediate bias is provided in the supplement figures (Figure S3).

4.5 Case E: Joint state-parameter estimation

Fig.9 presents the results for state-parameter estimation in phase diagrams. Fig.10 presents the PDF distribution of the phase diagrams. Not surprisingly, joint state-parameter estimation (Fig.9 a-e improves the posterior distribution compared to the case of state estimation (Fig.9 f-j.

The parameter estimate gradually reaches nearly its true value after a certain time period. In the state-parameter estimation case, the parameter estimate gradually changes from its prior, biased, value towards the correct estimate of $\epsilon = 0.7$ and remains at that value after that. Hence, in this case, the state variables are improved in the next seismic cycle which is not the case in state estimation. From this we can conclude that joint state-parameter estimation is in this case the most effective approach for seismic cycle estimation in the presence of a parameter bias. It is important to note that the state-parameter estimate does not only lead to a reasonably good posterior estimate of the state at these selected time steps, but at all assimilation time steps in the period considered, i.e., from $t = 4$ to $t = 500$ (Fig.4).
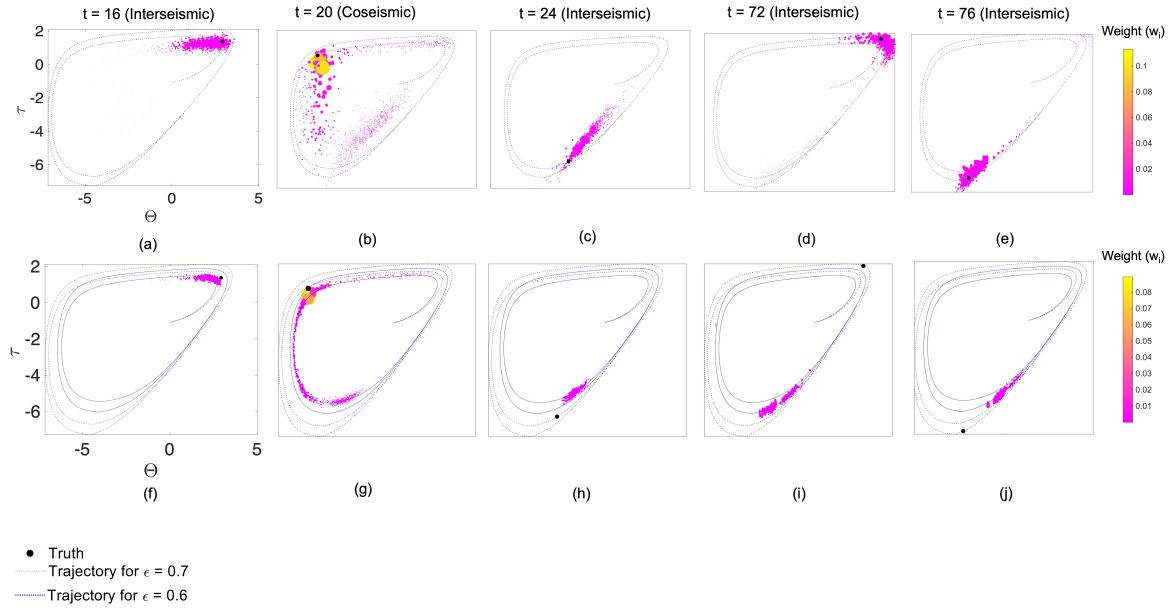
Figure 9. $\Theta - \tau$ phase diagrams for the case with (a-e) state-parameter estimation and (f-j) state estimation for intermediate bias. Use of colors and lines is the same as in Fig. 6.
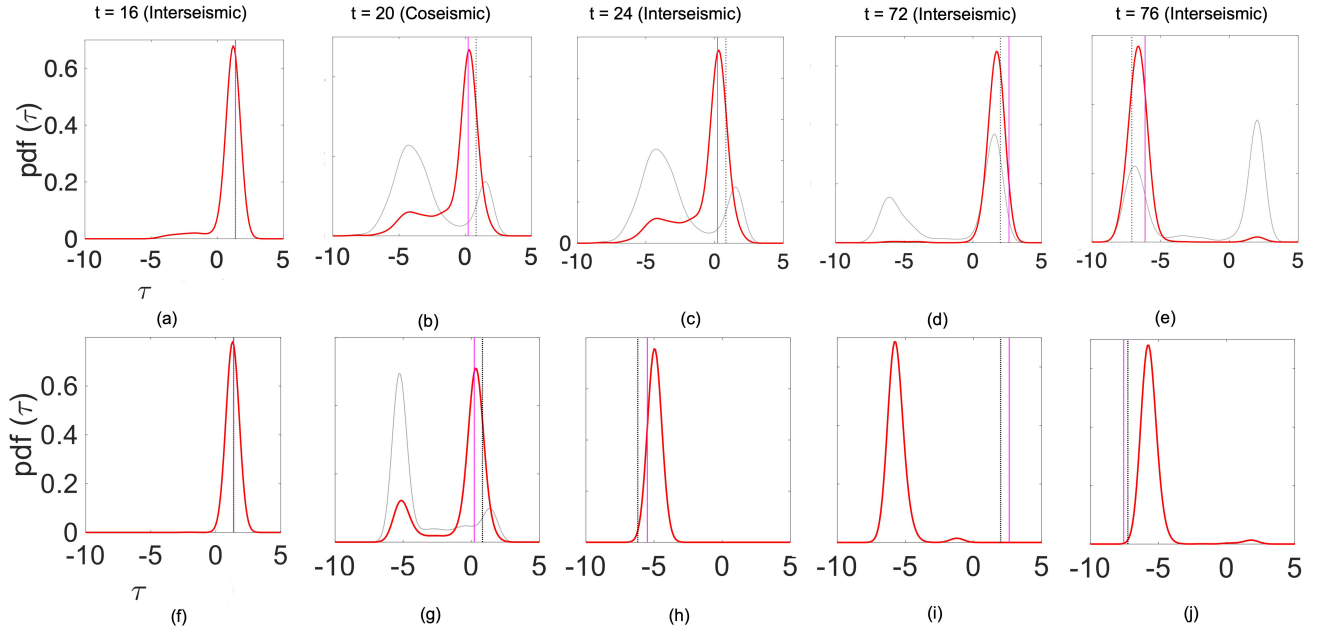
Figure 10. Corresponding PDFs for the case with (a-e) joint state-parameter estimation and (f-j) state estimation with intermediate bias in Fig. 9.

295   To evaluate the overall accuracy of the state- and the joint state parameter estimation for the different biased-parameter cases, we perform a regression analysis. The results in Fig.11 show how close the posterior estimates of the different experiments are to the truth using the R-squared (R^2) value. We find that when the parameter bias is small, state estimation is efficient with an R^2 value of 0.99. For the case of the intermediate bias, the setting of increasing the model error to 0.1 and consequent resampling with a smaller model error of std 0.01, results in an R^2 value of 0.61. However, for all of the cases, the joint state-

300   parameter estimation leads to significantly higher R^2 values and hence improved state estimates compared to the cases with state estimation only. This confirms our conclusion from section 4.5.
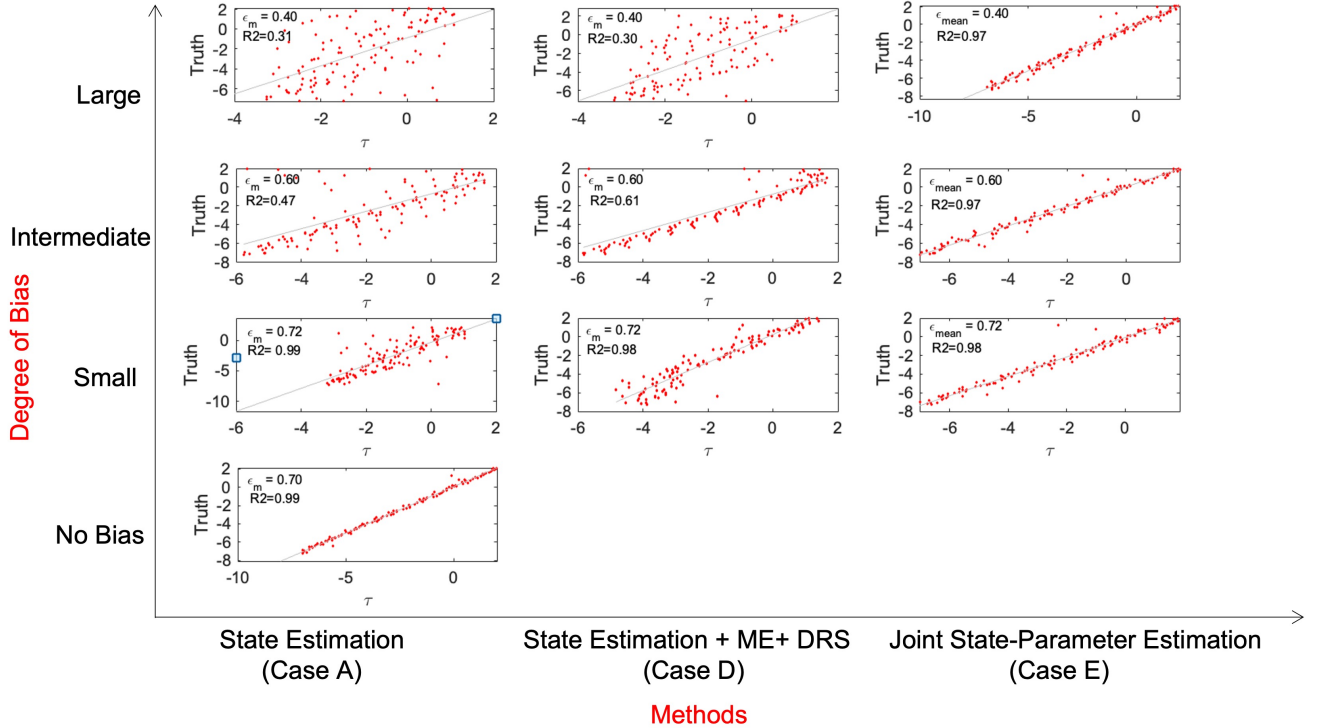
Figure 11. Comparison of regression between the estimate of τ and the true τ and the corresponding R^2 values for the three bias cases (rows) and for different assimilation approaches (columns). The red dots indicate the estimated values or the posterior and true τ values at the observation times. A diagonal line is added for reference.

5   Discussion

The results of this study illustrate the implications of parameter bias in data-assimilation applications for seismic-cycle modeling. They show it is feasible to apply a particle filter to a fault slip model. Moreover, they reveal that uncertainties in friction

305   parameters can be accounted either via directly estimating these parameters or via a larger model error. Accounting for these improved parameter estimates, also fault state estimates can be improved. This demonstrates that a possible trade-off between

estimating shear stress and friction can be effectively accounted for using data assimilation methods. In other words, data assimilation is able to separate error contributions due to uncertainties in friction (i.e., shear over normal stress) from uncertainties in estimates of a fault's shear stresses. This suggests that potentially large uncertainties in friction do not hamper the further development in directions using data assimilation methods or for physics-based seismic hazard assessment.

The simplest and most effective approach to deal with parameter bias, depends on the degree of parameter bias observed. For laboratory experiments with increased accuracy, one can potentially still use and tune state estimation, e.g., through increasing model error. However, for observed uncertainties in laboratory experiments in Niemeijer and Vissers (2014), and particularly when also accounting uncertainties in in-situ conditions (e.g., effective pressure and thermal conditions and amount of displacement) and laboratory setup (e.g., sample type with or without gouge) as well, state-parameter estimation is clearly the best and the required approach. It is remarkable to observe that by accounting for state-parameter estimation, any degree of bias can be dealt with equally effectively (Figure 11). This suggests that even upon extrapolation to significantly larger biases, state-parameter estimation can be an effective solution for earthquake cycle problems.

It is important to remember that these findings are based on the performance of state update and state-parameter update algorithms for a simplified nonlinear physics-based model in synthetic experiments. Some limitations that are still present in this pioneering study, which eventually need to be addressed, include:

- In this study, we assimilate both the fault shear stress and the slip rate observations on the plate interface. However, we have also conducted experiments with only assimilating the fault shear stress observations. It is observed in this case that the state estimate yields better fitting to the truth compared to the case when we assimilate both types of observations or only the slip rate. Assimilating slip-rate observations leads to lower weight values owing to their relatively high observation error. This affects the posterior estimate. However, a thorough study still needs to be conducted to identify which observations provide the most meaningful information when assimilated in earthquake-cycle models.

- In this study, we focus only on the uncertainty with respect to parameter ϵ. It can be seen from Eq.13, 14 and 15 that also the highly uncertain characteristic slip length L impacts fault states and cycle characteristics.

- Typically, earthquake forecasting is approached in a probabilistic manner (e.g. Marzocchi et al., 2017). Kinematic inversions of earthquake global positioning system (GPS) data have been used to estimate frictional properties in afterslip areas (e.g. Miyazaki et al., 2004; Hsu et al., 2006), but not for estimation of the earthquake dynamics themselves. As outlined by Van Dinther et al. (2019), data assimilation for earthquake sequences has the advantage that it can take into account measurement and model errors, non-Gaussian probabilities and sequential updating as data becomes available. The results of this study demonstrate how, for a highly simplified representation of earthquake cycles, non-linear data assimilation provides a means to account for both measurement errors and parameter biases. It also highlights how observations can be included as they become available. While particle filters are not computationally efficient, they can propagate the full error distribution which makes them attractive for estimation and forecasting of highly nonlinear processes like earthquake generation.

- Another point of attention is the selection of the number of particles required for a correct sampling of the prior. On the one hand, increasing the number of particles can improve estimation accuracy, but limited computational resources can make this impractical. On the other hand, having lower number of particles increase the risk of filter degeneracy. In this study, we initially used 50 and 100 particles, but increased the number of particles to 1000 to avoid degeneracy. Realization of 1000 particles may be computationally expensive for models that are more complex than the model used here. Improved sampling techniques, for example using a proposal density function, or using a particle flow (e.g. Hu and Van Leeuwen, 2021) could help to reduce computational costs while maintaining the advantage of a nonlinear filtering method.

- An additional point worth mentioning is the use of synthetic observations for fault displacement and velocities for data assimilation in this study. In realistic applications, the assumptions that we have considered with respect to data assimilation frequency and the standard deviation and distribution of the observational errors may not be valid. However, if we know the distribution of the measurement errors, we can use that information in choosing the relevant likelihood function that can greatly effect our fault estimates. Fault shear stress observations are usually not available, and if they are, they are subject to large errors. In contrast, fault velocities can be observed fairly accurately using GPS, as discussed by Van Dinther et al. (2019) who demonstrate that stress measurements are useful despite of their large errors. Following Van Dinther et al. (2019), we emphasize the need for conducting additional sensitivity studies to understand the implications of data gaps, outliers, and instrumental noise etc before our proposed methods can be used on real data.

- It is also very important to highlight the reason behind selecting a zero dimensional (0D) model for this study. Simplified fault slip models are computational efficient tools that help us to understand the physics behind the earthquake dynamics. A study by Li et al. (2021) compares the simulation of earthquakes in 0D, 1D, 2D, and 3D models and finds that lower-dimension models (0D and 1D) qualitatively represent the same dynamics as 2D and 3D models. Although 0D models cannot simulate the full complexity of the earthquake physics, they have the advantage that they are computationally inexpensive and provide the user with a tractable conceptual description of earthquake physics and the importance of the friction parameter. In our case, we were interested in investigating the effect of frictional parameter bias on the estimated fault states in earthquake cycle models. Hence in the present work, we investigated a simplified version of a Burridge-Knopoff spring-block slide model in a simplified 0D form. Eventually, to accurately simulate the behavior of real earthquake faults, 1D, 2D and 3D simulation models will be required (e.g., Li et al., 2021).

Nonetheless, simplified models provide useful insights to solve more complex problems. This is an important stepping stone to the development of data-assimilation applications for the simulation of more realistic earthquake cycles. Future developments for these purposes addressing the above limitations, could utilize other methods explicitly accounting for parameter-bias in the data-assimilation scheme to obtain a better accuracy (e.g., Dee and Da Silva, 1998; Sørensen and Madsen, 2004; Chepurin et al., 2005; Auligné et al., 2007; Li et al., 2009; Du et al., 2020).

6 Conclusions

In this study, we demonstrated the effect of a parameter bias in an earthquake cycle model on the estimated states with data assimilation. Synthetic, noisy observations of the shear stress and slip velocity on the fault plate interface were assimilated with state and state-parameter estimation methods using a particle filter. In our forward model, the shear-stress estimates strongly depend on the friction parameter ϵ. Therefore an inaccurate representation of this parameter would impact the stress estimates and forecasted cycles obtained using this model. To quantify this impact, we considered three different magnitudes of biases with respect to the true parameter $\epsilon_t = 0.7$, i.e., (i) small bias (model parameter $\epsilon_m = 0.72$), (ii) intermediate bias (model parameter $\epsilon_m = 0.60$) and (iii) large bias (model parameter $\epsilon_m = 0.40$).

We find that for a small bias in friction parameter ϵ, state estimation is most effective ($R^2 = 0.99$ for the regression between estimated and true shear stress). In the case of an intermediate bias, state estimation alone is less effective ($R^2 = 0.47$). However, by increasing the prior model error and adding a second resampling step in the data assimilation approach, the results can be improved ($R^2 = 0.61$). Nonetheless, state-parameter estimation in this case is best ($R^2 = 0.97$). In the case of a large parameter bias, state-parameter estimation ($R^2 = 0.97$) is significantly more effective manner to reconstruct the true state than state estimation ($R^2 = 0.31$) or improved state estimation with combined adjustments ($R^2 = 0.30$). This suggests that state-parameter estimation using data assimilation could be an effective method to improve forecasts of frequently recurring fault slip events.

Data availability. The observations in the study were generated by simulation. Extra explanatory figures have been uploaded to the Supplement.

Acknowledgements. The contributions of FV and AB have been funded by the Delft Technology Fellowship of Delft University of Technology. This work contributes to the DeepNL InFocus project funded by NWO (DEEP.NL.2018.037). The work benefited from discussions with André Niemeijer of Utrecht University and Hamed Diab-Montero of Delft University of Technology.

References

Auligné, T., McNally, A., and Dee, D.: Adaptive bias correction for satellite data in a numerical weather prediction system, Quarterly Journal of the Royal Meteorological Society, 133, 631–642, 2007.

395 Barbot, S., Lapusta, N., and Avouac, J.-P.: Under the hood of the earthquake machine: Toward predictive modeling of the seismic cycle, Science, 336, 707–710, 2012.

Bertino, L., Evensen, G., and Wackernagel, H.: Sequential data assimilation techniques in oceanography, International Statistical Review, 71, 223–241, 2003.

Burridge, R. and Knopoff, L.: Model and theoretical seismicity, Bulletin of the seismological society of America, 57(3), 341–371, 1967.

400 Cartwright, J. H., Hernández-García, E., and Piro, O.: Burridge-Knopoff models as elastic excitable media, Physical Review Letters, 79, 527, 1997.

Chepurin, G. A., Carton, J. A., and Dee, D.: Forecast model bias correction in ocean data assimilation, Monthly Weather Review, 133, 1328–1342, 2005.

Daley, R.: Atmospheric Data Assimilation (Special Issue Data Assimilation in Meteorology and Oceanography: Theory and Practice), Journal

405 of the Meteorological Society of Japan. Ser. II, 75, 319–329, 1997.

Dee, D. P. and Da Silva, A. M.: Data assimilation in the presence of forecast bias, Quarterly Journal of the Royal Meteorological Society, 124, 269–295, 1998.

Diab-Montero, H. A., Li, M., van Dinther, Y., and Vossepoel, F. C.: Estimating the occurrence of slow slip events and earthquakes with an Ensemble Kalman Filter, https://doi.org/https://doi.org/10.31223/X5135N, 2022.

410 Dieterich, J. H.: Modeling of rock friction: 1. Experimental results and constitutive equations, Journal of Geophysical Research: Solid Earth, 84, 2161–2168, 1979.

Doucet, A., De Freitas, N., and Gordon, N.: An introduction to sequential Monte Carlo methods, in: Sequential Monte Carlo methods in practice, pp. 3–14, Springer, 2001.

Du, M., Zheng, F., Zhu, J., Lin, R., Yang, H., and Chen, Q.: A New Ensemble-Based approach to correct the systematic ocean temperature bias

415 of CAS-ESM-C to improve its simulation and data assimilation abilities, Journal of Geophysical Research: Oceans, 125, e2020JC016 406, 2020.

Erickson, B., Birnir, B., and Lavallée, D.: A model for aperiodicity in earthquakes, Nonlinear processes in geophysics, 15, 1–12, 2008.

Erickson, B., Birnir, B., and Lavallée, D.: Periodicity, chaos and localization in a Burridge–Knopoff model of an earthquake with rate-and-state friction, Geophysical Journal International, 187, 178–198, 2011.

420 Evensen, G., Vossepoel, F. C., and Van Leeuwen, P. J.: Data Assimilation Fundamentals: A Unified formulation for State and Parameter Estimation, Springer, https://doi.org/10.1007/978-3-030-96709-3, Open access, 2022.

Fakuda, J., Johnson, K., Larson, K., and SI, M.: Fault friction parameters inferred from the early stages of afterslip following the 2003 Tokachi-Oki earthquake, Geophysical research letters, 114(B4), B04 412, 2009.

Gu, J., Rice, J. R., Ruina, A., and Tse, S.: Slip motion and stability of a single degree of freedom elastic system with rate and state dependent

425 friction, Journal of the Mechanics and Physics of Solids, 32(3), 167–196, 1984.

Hirahara, K. and Nishikiori, K.: Estimation of frictional properties and slip evolution on a long-term slow slip event fault with the ensemble Kalman filter: numerical experiments, Geophysical Journal International, 62, 2074–2096, 2019.

Hol, J. D., Schon, T. B., and Gustafsson, F.: On resampling algorithms for particle filters, in: 2006 IEEE nonlinear statistical signal processing workshop, pp. 79–82, IEEE, 2006.

430 Hori, T., Miyazaki, S., Hyodo, M., and Nakata, Rand Yoshiyuki, K.: Earthquake forecasting system based on sequential data assimilation of slip on the plate boundary, Theoretical and Applied Mechanics Japan, 62, 179–189, 2014.

Hsu, Y.-J., Simons, M., Avouac, J.-P., Galetzka, J., Sieh, K., Chlieh, M., Natawidjaja, D., Prawirodirdjo, L., and Bock, Y.: Frictional afterslip following the 2005 Nias-Simeulue earthquake, Sumatra, Science, 312, 1921–1926, 2006.

Hu, C.-C. and Van Leeuwen, P. J.: A particle flow filter for high-dimensional system applications, Q J R Meteorol Soc,
435 https://doi.org/10.1002/qj.4028, 2021.

Kalnay, E.: Atmospheric modeling, data assimilation and predictability, Cambridge university press, 2003.

Kano, M., Miyazaki, S., Ishikawa, Y., Hiyoshi, Y., Ito, K., and Hirahara, K.: Estimation of frictional parameters and initial values of simulation variables using an adjoint data assimilation method with synthetic afterslip data, Zishin 2, 63, 57–69, 2010.

Kano, M., Miyazaki, S., Ito, K., and Hirahara, K.: An adjoint data assimilation method for optimizing frictional parameters on the afterslip
440 area, Earth, Planets and Space, 65, 1575–1580, https://doi.org/10.5047/eps.2013.08.002, 2013.

Lapusta, N. and Barbot, S.: Models of earthquakes and aseismic slip based on laboratory-derived rate and state friction laws, The mechanics of faulting: From laboratory to real earthquakes, 661, 153–207, 2012.

Lapusta, N., Rice, J. R., Ben-Zion, Y., and Zheng, G.: Elastodynamic analysis for slow tectonic loading with spontaneous rupture episodes on faults with rate-and state-dependent friction, Journal of Geophysical Research: Solid Earth, 105, 23 765–23 789, 2000.

445 Li, H., Kalnay, E., Miyoshi, T., and Danforth, C. M.: Accounting for model errors in ensemble data assimilation, Monthly Weather Review, 137, 3407–3419, 2009.

Li, M., Pranger, C., and Van Dinther, Y.: Characteristics of earthquake cycles: a cross-dimensional comparison of 1D to 3D simulations, Submitted to Journal of Geophys. Res., Solid Earth, https://doi.org/10.1002/essoar.10509020.2, 2021.

Llenos, A. L. and McGuire, J. J.: Detecting aseismic strain transients from seismicity data, Journal of Geophysical Research: Solid Earth,
450 116, 2011.

Marone, C.: Laboratory-derived friction laws and their application to seismic faulting, Annual Review of Earth and Planetary Sciences, 26, 643–696, 1998.

Marzocchi, W., Taroni, M., and Falcone, G.: Earthquake forecasting during the complex Amatrice-Norcia seismic sequence, Science Advances, 3, e1701 239, https://doi.org/10.1126/sciadv.1701239, 2017.

455 Miyazaki, S.-i., Segall, P., Fukuda, J., and Kato, T.: Space time distribution of afterslip following the 2003 Tokachi-oki earthquake: Implications for variations in fault zone frictional properties, Geophysical Research Letters, 31, 2004.

Mowafy, A. E. and Bilbas, E.: Quality control in using GNSS CORS network for monitoring plate tectonics: a Western Australia case study, Journal of Survey Engineering, 142(2), 05015 003–(1–9), 2016.

Nakatani, M.: Conceptual and physical clarification of rate and state friction: Frictional sliding as a thermally activated rheology, Journal of
460 Geophysical Research: Solid Earth, 106, 13 347–13 380, 2001.

Niemeijer, A. and Vissers, R.: Earthquake rupture propagation inferred from the spatial distribution of fault rock frictional properties, Earth and Planetary Science Letters, 396, 154–164, 2014.

Rice, J. R. and Tse, S. T.: Dynamic motion of a single degree of freedom system following a rate and state dependent friction law, Journal of Geophysical Research: Solid Earth, 91, 521–530, 1986.

465 Ruina, A.: Slip instability and state variable friction laws, Journal of Geophysical Research: Solid Earth, 88(B12), 10 359–10 370, 1983.

Snyder, C., Bengtsson, T., Bickel, P., and Anderson, J.: Obstacles to high-dimensional particle filtering, Monthly Weather Review, 136, 4629–4640, 2008.

Sørensen, J. V. T. and Madsen, H.: Data assimilation in hydrodynamic modelling: on the treatment of non-linearity and bias, Stochastic Environmental Research and Risk Assessment, 18, 228–244, 2004.

470 Van Dinther, V., Kunsch, H. R., and Fichtner, A.: Ensemble data assimilation for earthquake sequences: Probabilistic estimation and forecasting of fault stresses, Geophysical Journal International, 217, 1453–1478, 2019.

Van Leeuwen, P. J.: Particle filtering in geophysical systems, Monthly Weather Review, 137, 4089–4114, 2009.

Van Leeuwen, P. J.: Representation errors and retrievals in linear and nonlinear data assimilation, Quarterly. J. Roy. Meteorol. Soc., 141, 1612–1623, https://doi.org/10.1002/qj.2464, 2015.

475 Vossepoel, F. C. and van Leeuwen, P. J.: Parameter estimation using a particle method: Inferring mixing coefficients from sea level observations, Monthly Weather Review, 135, 1006–1020, 2007.

Werner, M., Ide, K., and Sornette, D.: Earthquake forecasting based on data assimilation: Sequential Monte Carlo methods for renewal point processes, Nonlinear Processes in Geophysics, 18, 49–70, 2011.